

Spiral multiferroics as a natural skyrmion racetrack

Luca Maranzana,^{1,2} Maxim Mostovoy,³ Naoto Nagaosa,^{4,5} and Sergey Artyukhin¹

¹*Quantum Materials Theory, Italian Institute of Technology, Via Morego 30, Genoa, Italy*

²*Department of Physics, University of Genoa, Via Dodecaneso 33, Genoa, Italy*

³*Zernike Institute for Advanced Materials, University of Groningen,
Nijenborgh 3, 9747 AG Groningen, Netherlands*

⁴*RIKEN Center for Emergent Matter Science (CEMS), Wako, Saitama 351-0198, Japan*

⁵*Fundamental Quantum Science Program,
TRIP Headquarters, RIKEN, Wako 351-0198, Japan*

Abstract

Magnetic skyrmions are particle-like spin textures with a nontrivial topology, which ensures their stability even at the nanometer scale. This feature establishes skyrmions as promising information carriers for novel magnetic storage and processing devices, e.g., racetrack memories. However, their fate in various magnetic backgrounds is poorly understood. Here, we show that spiral multiferroics, some of the simplest noncollinear magnets, host bimerons—skyrmionic textures formed by vortex-antivortex pairs. The bimeron carries magnetic and ferroelectric dipole moments that remarkably depend on its position relative to the spiral background. This property enables precise positioning of the bimeron using a slowly rotating magnetic field, as a 2π field rotation shifts the bimeron by one spiral period. We also investigate the non-adiabatic regime that occurs when the rotation frequency exceeds a critical threshold. The results establish a new paradigm in which the background endows topological spin textures with unique functionalities, highlighting spiral multiferroics as a natural skyrmion racetrack.

INTRODUCTION

Localized topological defects in magnetic materials have attracted enormous interest and recently gave birth to the field of skyrmionics [1–4]. Magnetic skyrmions are nanometer-sized topologically stable spin textures that hold promise for new efficient information storage and processing devices, such as skyrmion racetrack memories [5, 6]. While skyrmions are usually studied on a ferromagnetic background, spiral multiferroics provide the simplest noncollinear background that breaks translation and inversion symmetries (see Fig. 1(a)) [7–9], leading to improper ferroelectricity, nonlocal domain wall dynamics and pinning [10–12]. Here, we show that spiral multiferroics host bimerons, skyrmion-like localized topological defects consisting of vortex-antivortex pairs (see Fig. 1(b, c)) [13–18]. These spin textures carry both magnetic and ferroelectric dipole moments, allowing their manipulation through electric and magnetic fields. The dynamics of bimerons on a spiral background is a problem of both fundamental and technological importance, as the interaction between the bimeron and the spiral results

in novel mechanisms for the manipulation of skyrmionic textures.

In racetrack memories, the information is encoded in the spatial arrangement of localized topological defects. Therefore, having robust control over their positions is crucial for storing and processing information. Here, we demonstrate that bimerons can be precisely positioned on a spiral background by a rotating magnetic field, for example, due to a circularly polarized electromagnetic wave. In fact, the field acts directly on the bimeron position due to the screw symmetry of the background, in contrast to the resonant coupling via an intermediate mode proposed in the context of skyrmions and bimerons in ferromagnets [19–22]. Hence, a slowly rotating magnetic field realizes an Archimedean screw-like pump in which the bimeron moves along the spiral wave vector by one period for each full rotation of the field. The spiral does not need to move to achieve this pumping, unlike usual Archimedean screws [23, 24]. Thus, the mechanism proposed here is not affected by bulk pinning [11] and does not involve high-frequency resonances of spiral internal modes [23]. We examine how the sign of the exchange interaction between adjacent spin spiral chains affects bimeron motion. We also investigate the non-adiabatic pumping induced by a fast-rotating field and the dynamics perpendicular to the spiral wave vector originating from Berry phase contributions. The findings, based on symmetries of the spiral background, can be applied to a wide variety of spiral multiferroics.

BIMERONS ON A SPIRAL BACKGROUND

Consider the following Ginzburg-Landau free energy describing a centrosymmetric spiral magnet in two dimensions,

$$H_0 = \int dx dy \left(J_x \left[-Q^2 (\partial_x \mathbf{m})^2 + \frac{1}{2} (\partial_{xx}^2 \mathbf{m})^2 \right] + \frac{1}{2} |J_\perp| (\partial_y \mathbf{m})^2 + K_z m_z^2 \right), \quad (1)$$

where the unit vector $\mathbf{m}(x, y)$ is the direction of the magnetization. The term proportional to $J_x > 0$ induces a rotation of $\mathbf{m}(x, y)$ in space with the wave vector $\pm Q \hat{x}$. $J_\perp < 0$ describes a ferromagnetic interaction along y . We treat the antiferromagnetic case in the final section. $K_z > 0$ represents an easy xy -plane anisotropy. Hence, the minimum energy configurations are two spirals where \mathbf{m} rotates in the xy -plane with chirality $\chi = \pm 1$,

$$\mathbf{m}_\chi(x) = (\cos(Qx - \phi), \chi \sin(Qx - \phi), 0). \quad (2)$$

The phase ϕ describes a translation of the entire spiral along x . In what follows, we consider the spiral in which spins rotate counterclockwise as we move in the x -direction, i.e. $\chi = +1$.

Two-dimensional ferromagnets host metastable states classified by the topological charge

(skyrmion number) [1, 2]

$$q_{\text{top}} = \frac{1}{4\pi} \int dx dy \mathbf{m} \cdot [\partial_x \mathbf{m} \times \partial_y \mathbf{m}]. \quad (3)$$

For an easy-axis anisotropy, the topological defect with $q_{\text{top}} = 1$ is a skyrmion [1–3]. Instead, for an easy-plane anisotropy, it is a bimeron, namely a vortex-antivortex pair with opposite m_z at the centers of the two defects [13–18]. Remarkably, spiral states minimizing Eq. (1), as well as conical spiral states [17], also host bimerons. As illustrated in Fig. 1(b), a bimeron can be constructed by rotating the spins within the black box about the x -axis. The rotation angle increases from 0 at the top of the box to 2π at the bottom. Thus, the bimeron twists the spiral plane by 2π in the y -direction. To ensure continuity of the magnetization texture at the boundary of the box, its width along x must be π/Q , and the spin rotation axis must be parallel to the spins at the vertical boundaries. Hence, this axis changes to the y -axis as we move the box and, therefore, the bimeron by $\pi/(2Q)$ along the x -direction (see Fig. 1(c)). In general, the spin rotation axis is $\hat{e}_\varphi = (\cos \varphi, \sin \varphi, 0)$, where $\varphi = Q\bar{x} - \phi + \pi/2$ depends on the bimeron x -coordinate, \bar{x} . We observe that φ corresponds to the vortex helicity, namely the angle between the in-plane spin component and the radius vector from the vortex center. We encode the previous considerations into an Ansatz for the spin texture of a bimeron with

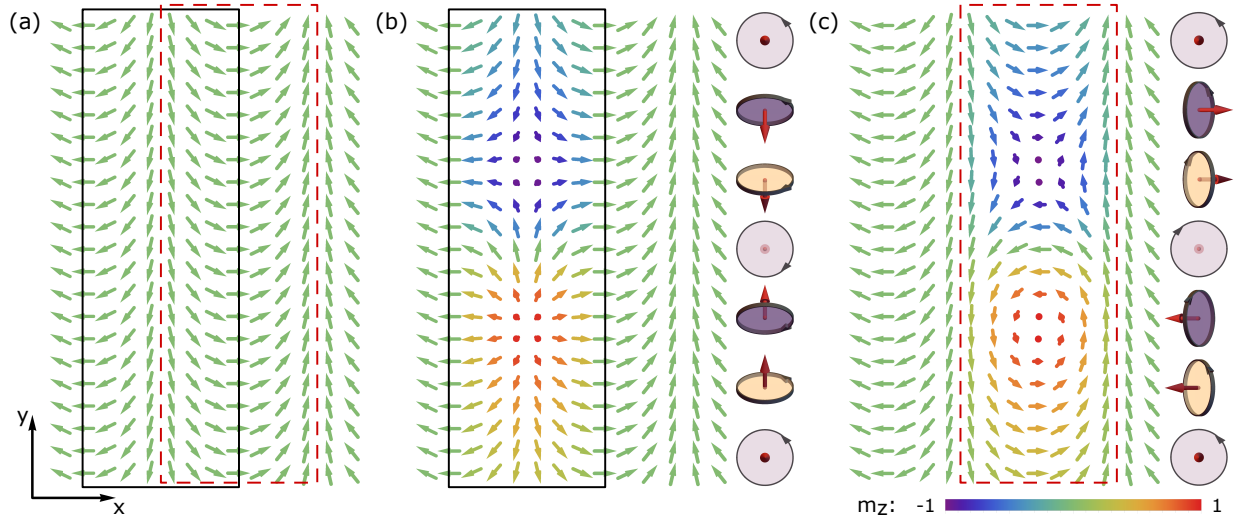


FIG. 1. (a) The spiral background breaks translational and rotational symmetries. Black and red boxes indicate the two stripes of width $\Delta x = \pi/Q$ at different positions relative to the spiral where the bimeron is inserted in panels (b) and (c). The colors encode the magnetization component m_z . The spiral plane rotates by -2π about \hat{x} , inside the black box (b), and about \hat{y} , inside the red box (c), upon moving along y , as shown on the right insets, resulting in a bimeron with helicity $\varphi = 0$ and $\varphi = \pi/2$, respectively. For either case, the bimeron consists of a vortex with positive m_z (red) and an antivortex with negative m_z (blue), each with topological charge $1/2$. Therefore, the total topological charge of the bimeron is 1.

position (\bar{x}, \bar{y}) :

$$\mathbf{m}(x, y) = \begin{cases} \hat{\mathcal{R}}_{\hat{e}_\varphi}(\theta(y - \bar{y})) \mathbf{m}_+(x) & -\frac{\pi}{2Q} < x - \bar{x} < \frac{\pi}{2Q}, \\ \mathbf{m}_+(x) & \text{otherwise} \end{cases}, \quad (4)$$

where $\mathbf{m}_+(x)$ is the counterclockwise spiral Eq. (2) and $\hat{\mathcal{R}}_{\hat{e}_\varphi}(\theta(y - \bar{y}))$ is a rotation matrix around \hat{e}_φ by an angle

$$\theta(y - \bar{y}) = 2q_{\text{top}} \arccos\left(\tanh\left(\frac{y - \bar{y}}{\tilde{\lambda}}\right)\right). \quad (5)$$

Minimizing Eq. (1) with respect to $\tilde{\lambda}$, we obtain $\tilde{\lambda} = \sqrt{3|J_\perp|/2K_z} \equiv \sqrt{3/2}\lambda$. The 2π twist of the spiral plane described by $\hat{\mathcal{R}}_{\hat{e}_\varphi}(\theta(y - \bar{y}))$ endows the bimeron with an integer topological charge $q_{\text{top}} = \pm 1$ and ensures its stability. We verify the latter property by relaxing the spin configuration Eq. (4) via the LLG dynamics [25–27] (see Appendix B).

The Ansatz Eq. (4) necessarily presents a derivative discontinuity in $\partial_x \mathbf{m}(x, y)$. Therefore, in what follows, we proceed with an Ansatz-free derivation of the general bimeron properties from its symmetries and length scales. The bimeron texture is invariant under the following two transformations of coordinates and spins:

$$x - \bar{x} \rightarrow -(x - \bar{x}) \quad \text{and} \quad (m_x, m_y) \rightarrow \hat{\mathcal{R}}_{\hat{z}}(2\varphi)(-m_x, m_y), \quad (6)$$

$$y - \bar{y} \rightarrow -(y - \bar{y}) \quad \text{and} \quad m_z \rightarrow -m_z, \quad (7)$$

where $\hat{\mathcal{R}}_{\hat{z}}(2\varphi)$ is a rotation matrix in the xy -plane by an angle 2φ , double the helicity angle.

Bimerons carry ferroelectric and magnetic dipole moments

$$d_z^{(E)} = \gamma \int dx dy (\hat{x} \cdot [\mathbf{m} \times \partial_y \mathbf{m}] - \hat{y} \cdot [\mathbf{m} \times \partial_x \mathbf{m}]) = C_E \frac{\gamma q_{\text{top}}}{Q} \sin(Q\bar{x} - \phi), \quad (8)$$

$$\mathbf{d}^{(M)} = \mu \int dx dy \mathbf{m} = -C_M \frac{\mu \lambda}{Q} (\cos(Q\bar{x} - \phi), \sin(Q\bar{x} - \phi), 0) \propto -\mathbf{m}_+(\bar{x}), \quad (9)$$

where γ is the magnetoelectric coupling constant [9], μ is the magnetic moment of a single spin, the bimeron length scales in the x and y directions are Q^{-1} and λ , and we imposed the constraint on φ discussed above. Using the Ansatz Eq. (4), we can estimate the dimensionless shape factors C_E and C_M : $C_E = \pi^2$ and $C_M = 4\sqrt{6}$. The components of $\mathbf{d}^{(M)}$ perpendicular to $\mathbf{m}_+(\bar{x})$ are zero due to Eq. (6) and Eq. (7). Similarly, $\hat{y} \cdot [\mathbf{m} \times \partial_x \mathbf{m}]$ does not contribute to the integral, because of Eq. (7). Remarkably, the dipole moments depend on the bimeron position \bar{x} . In particular, $\mathbf{d}^{(M)}$ is opposite to the magnetization of the spiral background at the bimeron center, $\mathbf{m}_+(\bar{x})$. Bimerons also carry an electric dipole moment in the y -direction $d_y^{(E)} = \gamma \int dx dy (\hat{z} \cdot [\mathbf{m} \times \partial_x \mathbf{m}] - \hat{z} \cdot [\mathbf{m}_+ \times \partial_x \mathbf{m}_+])$, as spins near the bimeron center rotate

with the opposite chirality with respect to the spiral background $\mathbf{m}_+(x)$. Hence, the bimeron constitutes the smallest ferroelectric domain in spiral multiferroics. However, $d_y^{(E)}$ does not affect the dynamics described in this work since it is independent of the bimeron position.

Using Eq. (8) and Eq. (9), the bimeron energy in the presence of an electric field E_z and a magnetic field \mathbf{H} takes the form, at the first order in the applied fields,

$$H = H_0 - C_E \frac{\gamma q_{\text{top}}}{Q} E_z \sin(Q\Delta\bar{x}) + C_M \frac{\mu\lambda}{Q} \mathbf{H} \cdot (\cos(Q\Delta\bar{x}), \sin(Q\Delta\bar{x}), 0) \equiv H_0 + U_{\Delta\bar{x}}, \quad (10)$$

where $\Delta\bar{x} = \bar{x} - \phi/Q$ is the bimeron position relative to the spiral background. The applied fields favor a specific position for the bimeron, modulo the spiral period $2\pi/Q$. This result is closely connected to the screw symmetry of the background: the spiral in Eq. (2) is invariant under the combined action of a rotation of \mathbf{m} in the xy -plane by an angle ϕ and a translation along x by ϕ/Q . Hence, $\Delta\bar{x}$ must involve both translation and rotation to move the bimeron along x without altering the spiral background. At zero applied fields, the energy Eq. (1) is invariant under these two transformations. Consequently, the bimeron can freely move with respect to the spiral background. However, the applied fields break isotropy in the xy -plane and, therefore, the symmetry associated with $\Delta\bar{x}$. The bimeron now experiences a potential $U_{\Delta\bar{x}}$ that depends on its position relative to the spiral $\Delta\bar{x}$. In-plane anisotropy also breaks rotational symmetry and contributes to $U_{\Delta\bar{x}}$. For simplicity, we first focus on the effects of the fields and cover in-plane anisotropy in the final section.

ARCHIMEDEAN SCREW-LIKE PUMP FOR BIMERONS

Consider the rotating magnetic field $\mathbf{H}(t) = |\mathbf{H}| (\cos(\omega t), \sin(\omega t), 0)$, for example, due to a circularly polarized electromagnetic wave propagating in the z -direction. Its contribution to the bimeron energy Eq. (10) takes the form $U_{\Delta\bar{x}} \propto \cos(Q\Delta\bar{x} - \omega t)$, a sinusoidal potential that moves with velocity ω/Q . For a slowly rotating field, the bimeron adiabatically follows one of the minimums of the potential $\Delta\bar{x}_{\text{min}}^{(n)} = (\omega/Q)t + (2n+1)\pi/Q$ with $n \in \mathbb{Z}$ and, thus, moves along x by one spiral period for each full rotation of the magnetic field (see Fig. 2(a)), resembling the Archimedean screw. In contrast to the typical realization of this mechanism [23, 24], the spiral does not need to move since the bimeron is pumped relative to it.

To describe the motion along y and the non-adiabatic regime of this bimeron Archimedean pump, we consider the following Lagrangian and Rayleigh dissipation functional that encode the dynamics of a magnetization texture $\mathbf{m}(t, \mathbf{r})$ [25, 26, 28],

$$L = \int dx dy \mathbf{A}(\mathbf{m}) \cdot \dot{\mathbf{m}} - H, \quad R = \frac{\alpha}{2} \int dx dy \dot{\mathbf{m}}^2, \quad (11)$$

where the Berry connection $\mathbf{A}(\mathbf{m})$ satisfies $\nabla_{\mathbf{m}} \times \mathbf{A}(\mathbf{m}) = \mathbf{m}$, the gyromagnetic ratio is set to 1, and $\alpha \ll 1$ denotes the Gilbert damping constant.

The dynamics described by Eq. (11) can be solved exactly only in the simplest cases [29]. Thus, we apply the collective coordinates approach [30, 31]. In this framework, the dynamics of a magnetization texture is formulated in terms of the collective coordinates $\xi_I(t)$, so that $\mathbf{m}(t, \mathbf{r}) = \mathbf{m}(\{\xi_I(t)\}, \mathbf{r})$. Although $\mathbf{m}(t, \mathbf{r})$ possess infinitely many $\xi_I(t)$, only the *soft* modes with low characteristic frequencies, compared to the timescales of the dynamics, are relevant. The other *hard* modes adiabatically adjust to their equilibrium values. Here, we explore the dynamics induced by a magnetic field that rotates significantly slower than the characteristic frequencies determined by Eq. (1), e.g. $\omega_{\text{res}} = \sqrt{10K_z J_x Q^4}$ that corresponds to the resonant sliding of the spiral background [23]. Hence, only the modes associated with the continuous symmetries of Eq. (1)— $\Delta\bar{x}(t)$, $\bar{y}(t)$ and $\phi(t)$ —can be excited. The spiral phase $\phi(t)$ and the bimeron y -coordinate $\bar{y}(t)$ correspond to global translations along x and y : $\partial_\phi = -(1/Q)\partial_x$ and $\partial_{\bar{y}} = -\partial_y$. The bimeron x -coordinate relative to the spiral background $\Delta\bar{x}(t)$ moves the bimeron along x without altering the spiral, as it involves the screw symmetry discussed at the end of the previous section.

Substituting $\mathbf{m}(t, \mathbf{r}) = \mathbf{m}(\{\xi_I(t)\}, \mathbf{r})$ in Eq. (11), one obtains an effective Lagrangian and Rayleigh dissipation functional, where the dynamical variables are only the soft modes $\xi_I(t)$. The corresponding equations of motion take the form [30, 31]

$$\alpha\Gamma_{IJ}\dot{\xi}_J - G_{IJ}\dot{\xi}_J = F_I, \quad (12)$$

where I and J run over the soft modes, $\Delta\bar{x}(t)$, $\bar{y}(t)$ and $\phi(t)$. The damping matrix $\Gamma_{IJ} = \Gamma_{JI}$, the gyrotropic matrix $G_{IJ} = -G_{JI}$ and the conservative forces F_I acting on ξ_I descend from

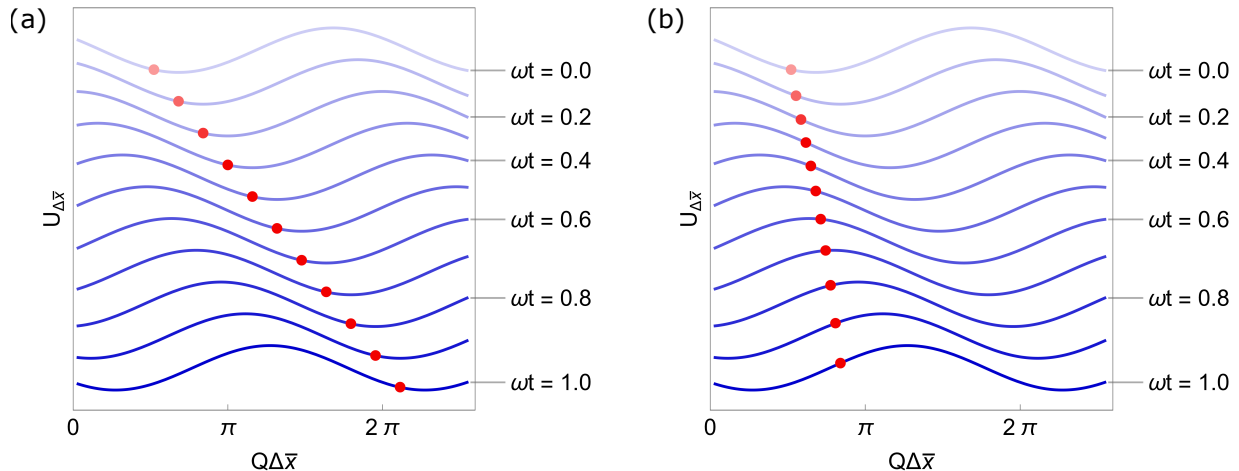


FIG. 2. Effective potential induced by the rotating magnetic field $U_{\Delta\bar{x}}$ as a function of the bimeron position relative to the spiral background $\Delta\bar{x}$, plotted at different times t . (a) For a slowly rotating field, the bimeron (red dot) follows the sliding potential $U_{\Delta\bar{x}}$, residing near a minimum. (b) Above a critical rotation frequency, the bimeron is no longer confined within a well of $U_{\Delta\bar{x}}$ because of the gyrotropic and damping forces.

R , $\mathbf{A}(\mathbf{m}) \cdot \dot{\mathbf{m}}$ and H , respectively. In Appendix A, we derive these terms for a bimeron under the action of a rotating magnetic field.

For large systems, with size $L_x L_y \gg \lambda/(Q\alpha^2)$, the velocity of the spiral $v_s = \dot{\phi}/Q$ becomes

$$v_s = -\frac{16\pi^2}{C_{\bar{y}}} \frac{\lambda}{Q\alpha^2 L_x L_y} \Delta\dot{\bar{x}}. \quad (13)$$

Using the Ansatz Eq. (4), we can estimate the dimensionless shape factor $C_{\bar{y}}$: $C_{\bar{y}} = 4\pi\sqrt{2/3}$. As the bimeron moves relative to the spiral with a velocity $\Delta\dot{\bar{x}}$, the entire spiral background moves in the opposite direction. Since the spiral experiences a damping proportional to the system size, its velocity $v_s \propto (L_x L_y)^{-1}$ is negligible with respect to the bimeron velocity $\Delta\dot{\bar{x}}$. Within this approximation, the other two equations resulting from Eq. (12) take the form

$$\Delta\dot{\bar{x}} = \frac{\alpha\mu C_{\bar{y}} C_M}{16\pi^2 Q} |\mathbf{H}| \sin(Q\Delta\bar{x} - \omega t), \quad \dot{\bar{y}} = -\frac{4\pi q_{\text{top}} Q \lambda}{\alpha C_{\bar{y}}} \Delta\dot{\bar{x}}. \quad (14)$$

The bimeron moves along y , perpendicular to the spiral wave vector, with a velocity $\dot{\bar{y}}$ that is proportional to the velocity along x , $\Delta\dot{\bar{x}}$, and to the topological charge, q_{top} . This result can be explained considering each term in Eq. (12) as a force. The gyrotropic term, proportional to G_{IJ} , results in the ‘‘Lorentz’’ force $\mathbf{F}_G \propto q_{\text{top}} \mathbf{v}_b \times \hat{z}$, where \mathbf{v}_b is the bimeron velocity. As it moves in the x -direction, following the sliding potential due to the rotating magnetic field $U_{\Delta\bar{x}}$, the bimeron is pushed in the y -direction by \mathbf{F}_G . The resulting $\dot{\bar{y}}$ leads to a x -component of \mathbf{F}_G , which drives the bimeron away from the minimum of $U_{\Delta\bar{x}}$. This effect combines with the damping force $\mathbf{F}_\Gamma \propto -\alpha \mathbf{v}_b$ and, above a critical \mathbf{v}_b , overcomes the barrier that confines the bimeron in one of the wells of the sliding sinusoidal potential $U_{\Delta\bar{x}}$ (see Fig. 2(b)). Thus, the Archimedean pump enters a new dynamical regime where the bimeron no longer follows $U_{\Delta\bar{x}}$. To describe such a transition, we first seek a solution of the form $\Delta\bar{x} = (\omega/Q)t + \Delta x_0$, where the bimeron follows the sliding potential. The first of Eq. (14) becomes

$$1 \geq \sin(Q\Delta x_0) = \frac{16\pi^2 \omega}{\alpha\mu C_{\bar{y}} C_M |\mathbf{H}|} \implies \omega \leq \frac{\alpha\mu C_{\bar{y}} C_M |\mathbf{H}|}{16\pi^2} \equiv \omega^*. \quad (15)$$

This steady-state solution exists only if the rotation frequency of the magnetic field is below a critical threshold ω^* , which corresponds to the critical bimeron velocity $\Delta\dot{\bar{x}}^* = \omega^*/Q$. In such a case, the position of the bimeron relative to the sliding potential $U_{\Delta\bar{x}}$ takes the form $\Delta x_0 = ((2n+1)\pi - \arcsin(\omega/\omega^*))/Q$ with $n \in \mathbb{Z}$. Therefore, the bimeron is displaced from a minimum of the potential by $d = -\arcsin(\omega/\omega^*)/Q$, so that the conservative force exerted by $U_{\Delta\bar{x}}$ compensates for the gyrotropic and damping forces. At $\omega = \omega^*$, the displacement d corresponds to the steepest point of $U_{\Delta\bar{x}}$, and the conservative force is the maximum possible. Hence, at higher frequencies, the sliding potential can no longer confine the bimeron and no stationary solution exists. The time-averaged bimeron velocity along the x -direction \bar{v}_x still

takes a simple form, and we have (see Fig. 3)

$$\bar{v}_x = \Delta \dot{\tilde{x}} = \frac{\omega}{Q} \quad \text{for } \omega \leq \omega^*, \quad \bar{v}_x = \frac{\omega}{Q} \left(1 - \sqrt{1 - \frac{\omega^{*2}}{\omega^2}} \right) \quad \text{for } \omega > \omega^*. \quad (16)$$

To summarize, the rotating magnetic field with angular frequency ω induces a translation of the effective potential for the bimeron with a velocity ω/Q . For $\omega \leq \omega^*$, the bimeron follows the sliding potential. Consequently, its velocity increases linearly with ω and is remarkably independent of the field strength and Gilbert damping constant. This driving mechanism is an analog of the Archimedean screw, except for the fact that the spiral background remains fixed. At a critical angular frequency ω^* , proportional to the strength of the magnetic field, such an Archimedean screw breaks down due to the gyrotropic and damping forces, and the dynamics sharply enters a new regime where the bimeron velocity decreases as ω increases. The bimeron also moves perpendicular to the spiral wave vector with a velocity $\dot{\tilde{y}}$ inversely

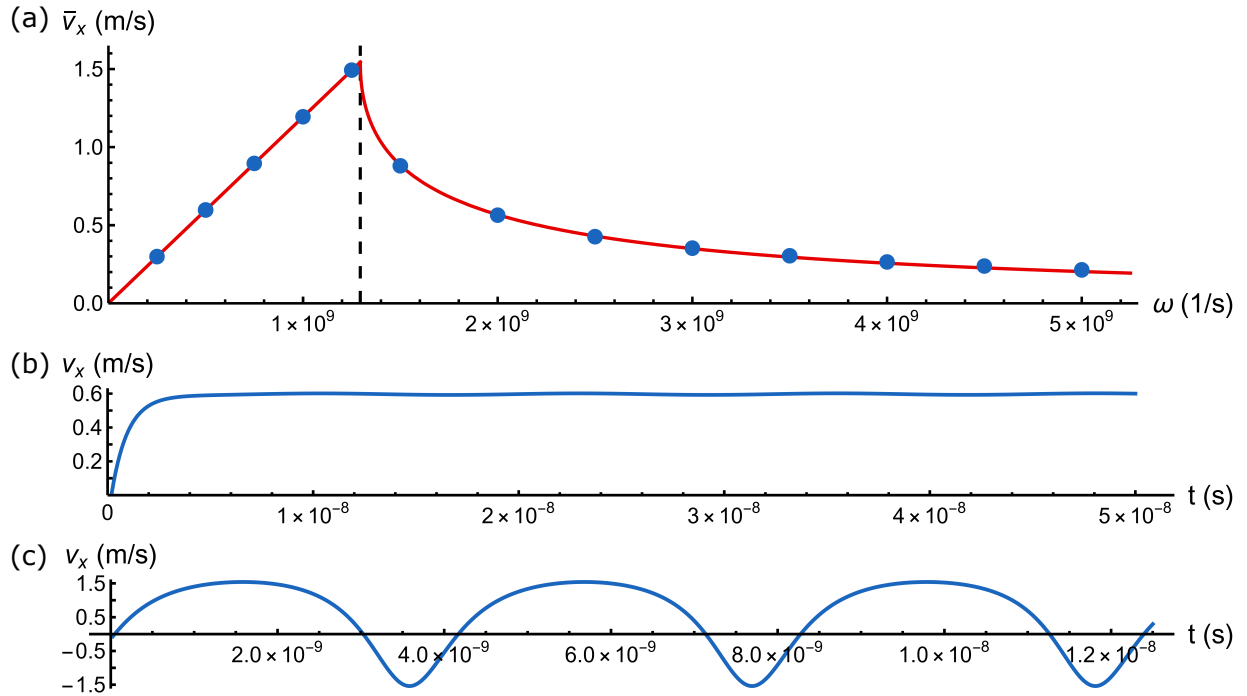


FIG. 3. (a) Time-averaged velocity \bar{v}_x of a bimeron moving under the action of a rotating magnetic field with angular frequency ω . Blue dots indicate the numerical result of the LLG equation [25–27] for $Q = 8.38 \cdot 10^8 \text{ m}^{-1}$, $|\mathbf{H}| = 0.1 \text{ T}$, $\alpha = 0.1$ and $\mu = \mu_B$, where μ_B is the Bohr magneton. The red line shows the analytical solution Eq. (16) with fitted critical angular frequency $\omega^* = 1.29 \cdot 10^9 \text{ s}^{-1}$. Using Eq. (15), we estimate ω^* analytically: $\omega^* = 1.12 \cdot 10^9 \text{ s}^{-1}$. Panels (b) and (c) show the bimeron velocity $v_x = \Delta \dot{\tilde{x}}$ as a function of time in the two dynamical regimes. (b) For $\omega = 5 \cdot 10^8 \text{ s}^{-1} < \omega^*$, v_x reaches the steady-state velocity after a transient in which the bimeron adjusts to its equilibrium position on the sliding potential shown in Fig. 2(a). (c) For $\omega = 2 \cdot 10^9 \text{ s}^{-1} > \omega^*$, v_x oscillates with a nonzero average \bar{v}_x , as the bimeron no longer follows a minimum of the potential (see Fig. 2(b)).

proportional to the Gilbert damping constant $\alpha \ll 1$ (see Eq. (14)). Therefore, \dot{y} dominates over $\Delta\dot{x}$, in contrast to the antiferromagnetic case treated in the final section. These results are expressed for a counterclockwise spin rotation in the spiral background Eq. (2), $\chi = +1$. In the clockwise case, $\chi = -1$, the velocity of the bimeron is opposite in sign. We corroborate the analytical solution with spin dynamics simulations [27] (see Fig. 3 and Appendix B).

Domain walls in easy-axis ferromagnets exhibit a behavior analogous to Eq. (16) under a rotating magnetic field in the hard-plane [32, 33]. The domain wall position x_{DW} and helicity φ_{DW} play the roles of the bimeron coordinates \bar{y} and $\Delta\bar{x} = (\varphi - \pi/2)/Q$, respectively. Thus, in contrast to the present case, the Archimedean screw pumps a purely rotational mode, the domain wall helicity φ_{DW} .

IN-PLANE ANISOTROPY

In the presence of in-plane anisotropy K_y , the following term must be added to the energy of a bimeron, Eq. (10):

$$H_{K_y} = \int dx dy K_y m_y^2 = -C_{K_y} K_y \frac{\lambda}{Q} \sin^2(Q\Delta\bar{x}). \quad (17)$$

With the Ansatz Eq. (4), the shape factor becomes $C_{K_y} = 2\pi\sqrt{2/3}$. Unlike the contribution of the rotating magnetic field, the potential in Eq. (17) is static and has half the period. For $|\mathbf{H}| < H^* = C_{K_y}|K_y|/C_M\mu$, the maximum force due to the field $F_{\text{max}}^{(\mathbf{H})} = C_M\mu\lambda|\mathbf{H}|$ is smaller than the one exerted by the anisotropy $F_{\text{max}}^{(K_y)} = C_{K_y}K_y\lambda$. Therefore, the bimeron is confined in one of the wells of the static potential in Eq. (17). When $|\mathbf{H}| > H^*$, the rotating magnetic field overcomes the anisotropy and sets the bimeron in motion. Since now the shape of the sliding potential changes over time, there is no longer a steady-state solution. Nevertheless, at low driving frequencies, the bimeron still follows a minimum of this potential. Hence, its average velocity in the x -direction is still ω/Q . That is, the bimeron Archimedean pump is robust against small in-plane anisotropy.

NÉEL BIMERON DYNAMICS

Thus far, we have considered materials with a ferromagnetic exchange J_{\perp} between neighboring spiral chains. When J_{\perp} is antiferromagnetic, the spin texture can be described by the Néel vector $\mathbf{n}(\mathbf{r}) = (\mathbf{m}_1(\mathbf{r}) - \mathbf{m}_2(\mathbf{r}))/2$ and the total magnetization $\mathbf{m}(\mathbf{r}) = \mathbf{m}_1(\mathbf{r}) + \mathbf{m}_2(\mathbf{r})$, where $\mathbf{m}_1(\mathbf{r})$ and $\mathbf{m}_2(\mathbf{r})$ are the magnetization fields in the two antiferromagnetic sublattices. Integrating out $\mathbf{m}(\mathbf{r})$, the Lagrangian and Rayleigh dissipation functional become

$$L_{\text{AF}} = \int dx dy \frac{1}{J_{\perp}} (\dot{\mathbf{n}}^2 - \mu\mathbf{H} \cdot \mathbf{n} \times \dot{\mathbf{n}}) - H_{\text{AF}}, \quad R_{\text{AF}} = \frac{\alpha}{2} \int dx dy \dot{\mathbf{n}}^2, \quad (18)$$

where \mathbf{H} is the applied magnetic field, and the Ginzburg-Landau free energy for $\mathbf{n}(\mathbf{r})$ reads

$$H_{\text{AF}} = \int dx dy \left(J_x \left[-Q^2 (\partial_x \mathbf{n})^2 + \frac{1}{2} (\partial_{xx}^2 \mathbf{n})^2 \right] + \frac{1}{2} J_{\perp} (\partial_y \mathbf{n})^2 + K_z n_z^2 + \frac{\mu^2}{4J_{\perp}} (\mathbf{n} \cdot \mathbf{H})^2 \right). \quad (19)$$

At $\mathbf{H} = 0$, H_{AF} is formally identical to the Ginzburg-Landau free energy for a ferromagnetic J_{\perp} , Eq. (1). Hence, the structure of a \mathbf{n} -bimeron is the same as discussed for a \mathbf{m} -bimeron. However, the interaction with an applied magnetic field resembles quadratic anisotropy with a hard axis along \mathbf{H} . Thus, a static magnetic field $\mathbf{H}_{\text{static}} = (2\sqrt{J_{\perp}|K_y|/\mu}) \hat{e}$ can be applied to compensate for the effects of $K_y > 0$, with $\hat{e} = \hat{x}$, and $K_y < 0$, with $\hat{e} = \hat{y}$. The bimeron energy takes the form

$$H_{\text{AF}} = H_0^{(\text{AF})} - C_M^{(\text{AF})} \frac{\mu^2 \lambda}{4J_{\perp} Q} [\mathbf{H} \cdot (\cos(Q\Delta\bar{x}), \sin(Q\Delta\bar{x}), 0)]^2, \quad (20)$$

where the dimensionless shape factor $C_M^{(\text{AF})}$ coincides with $C_{K_y} = 2\pi\sqrt{2/3}$.

Consider now the dynamics driven by the rotating magnetic field. For $\omega \ll \mu|\mathbf{H}| \ll \alpha J_{\perp}$, the first terms in L_{AF} are negligible, and the equations of motion for the bimeron become

$$\Delta\dot{\bar{x}} = -\frac{\mu^2 |\mathbf{H}|^2 C_M^{(\text{AF})}}{4\alpha J_{\perp} C_{\Delta\bar{x}} Q} \sin(2(Q\Delta\bar{x} - \omega t)), \quad \dot{\bar{y}} = 0 + \mathcal{O}\left(\frac{\mu|\mathbf{H}|}{\alpha J_{\perp}}\right). \quad (21)$$

Using the Ansatz Eq. (4), we can estimate the dimensionless shape factor $C_{\Delta\bar{x}} = 10\pi\sqrt{2/3}$. In contrast to the ferromagnetic case (see Eq. (14)), the y -component of the bimeron velocity $\dot{\bar{y}}$ is negligible compared to the x -component $\Delta\dot{\bar{x}}$. Indeed, there is no gyrotropic force in the Néel vector dynamics. Nevertheless, bimeron motion still presents the two regimes described by Eq. (16), but now the critical rotation frequency is

$$\omega_{\text{AF}}^* = \frac{\mu^2 |\mathbf{H}|^2 C_M^{(\text{AF})}}{4\alpha J_{\perp} C_{\Delta\bar{x}}}. \quad (22)$$

Since ω_{AF}^* is due only to damping, it is inversely proportional to α . In contrast, the gyrotropic force dominates in the ferromagnetic case, and ω^* is directly proportional to α , Eq. (15).

CONCLUSIONS

We have shown that centrosymmetric spiral magnets host bimerons, localized topological spin textures similar to skyrmions, which carry magnetic and ferroelectric dipole moments. Remarkably, these dipole moments depend on the bimeron position with respect to the spiral background. Therefore, an electromagnetic field acts directly on the translational modes of this topological defect, in contrast to bimerons and skyrmions in ferromagnets. Specifically,

a slowly rotating magnetic field pumps bimerons along the spiral wave vector by one period for each full rotation of the field. This adiabatic pumping is robust against small perturbations, e.g. due to in-plane anisotropy. However, it breaks down if the magnetic field rotates faster than a critical threshold because of gyrotropic effects (i.e. Berry phase contributions) or damping. If adjacent spin-spiral chains interact ferromagnetically, the bimeron also moves perpendicular to the spiral wave vector with a velocity proportional to its topological charge. In contrast, topological charge contributions cancel between two antiferromagnetically interacting spin chains, and the bimeron only moves along the spiral wave vector. Since bimerons represent the smallest ferroelectric domains in spiral multiferroics, they can be nucleated by an applied electric field and inflated into larger bubbles, which second harmonic generation experiments could detect [34, 35]. We expect these bubble domains to be pumped similarly to bimerons under the action of a rotating magnetic field.

The results rely only on the symmetries of the spiral background and naturally extend to three-dimensional systems, for which the bimeron texture repeats for every fixed z , forming a bimeron string. Therefore, bulk spiral multiferroics, such as TbMnO_3 , MnWO_4 , and CuO [7, 36], are promising candidates for realizing an Archimedean screw-like pump for bimerons. In materials with strong easy-axis anisotropy, the rotating magnetic field has to overcome a significant energy barrier to pump the bimeron. However, this barrier can be suppressed by applying an additional static magnetic field, estimated at 4–8 T for MnWO_4 and TbMnO_3 . In bulk multiferroics, spins in adjacent spiral chains typically interact antiferromagnetically. In contrast, monolayer multiferroics exhibit ferromagnetically coupled spiral chains, e.g. VI_2 , NiI_2 , and NiBr_2 [37, 38]. Hence, both the dynamical cases can be accessed. Nevertheless, the antiferromagnetic case is probably more relevant for racetrack memory applications, as the bimeron moves along a fixed direction, the spiral wave vector. Thus, bulk spiral multiferroics realize a natural racetrack, where a 2π field rotation shifts skyrmionic textures by precisely one spiral period.

ACKNOWLEDGMENTS

N.N. was supported by JSPS KAKENHI Grant Numbers 24H00197 and 24H02231. N.N. was supported by the RIKEN TRIP initiative.

APPENDIX A: COLLECTIVE COORDINATES APPROACH

The damping matrix, the gyrotropic matrix, and the conservative forces entering Eq. (12) take the form [30, 31]

$$\Gamma_{IJ} = \int dx dy \frac{\partial \mathbf{m}}{\partial \xi_I} \cdot \frac{\partial \mathbf{m}}{\partial \xi_J}, \quad G_{IJ} = \int dx dy \mathbf{m} \cdot \left[\frac{\partial \mathbf{m}}{\partial \xi_I} \times \frac{\partial \mathbf{m}}{\partial \xi_J} \right], \quad F_I = -\frac{\partial H}{\partial \xi_I}. \quad (23)$$

The bimeron symmetries Eq. (6) and Eq. (7) result in $\Gamma_{\Delta\bar{x}\bar{y}} = \Gamma_{\phi\bar{y}} = G_{\Delta\bar{x}\phi} = 0$. Combining the definition of topological charge Eq. (3) with the relation between mode-derivatives and coordinate-derivatives, we get $G_{\Delta\bar{x}\bar{y}} = 4\pi q_{\text{top}}$ and $G_{\phi\bar{y}} = 4\pi q_{\text{top}}/Q$. Neglecting the bimeron contribution over the spiral one, we obtain $\Gamma_{\phi\phi} = L_x L_y$, where $L_x L_y$ is the area of the system. Thus, the damping matrix Γ_{IJ} and the gyrotropic matrix G_{IJ} take the form ($I, J = \Delta\bar{x}, \bar{y}, \phi$)

$$\Gamma_{IJ} = \begin{pmatrix} Q\lambda C_{\Delta\bar{x}} & 0 & \lambda C_{\Delta\bar{x}\phi} \\ 0 & C_{\bar{y}}/Q\lambda & 0 \\ \lambda C_{\Delta\bar{x}\phi} & 0 & L_x L_y \end{pmatrix}, \quad G_{IJ} = \begin{pmatrix} 0 & 4\pi q_{\text{top}} & 0 \\ -4\pi q_{\text{top}} & 0 & -4\pi q_{\text{top}}/Q \\ 0 & 4\pi q_{\text{top}}/Q & 0 \end{pmatrix}, \quad (24)$$

where $C_{\Delta\bar{x}}$, $C_{\bar{y}}$ and $C_{\Delta\bar{x}\phi}$ are dimensionless shape factors. Using the Ansatz Eq. (4), we can estimate such factors, obtaining $C_{\Delta\bar{x}} = 10\pi\sqrt{2/3}$, $C_{\bar{y}} = 4\pi\sqrt{2/3}$ and $C_{\Delta\bar{x}\phi} = 2\pi\sqrt{6}$. While $F_{\bar{y}} = F_{\phi} = 0$ due to translational symmetry, the conservative force acting on $\Delta\bar{x}$ is

$$F_{\Delta\bar{x}} = C_E \gamma q_{\text{top}} E_z \cos(Q\Delta\bar{x}) + C_M \mu \lambda \mathbf{H} \cdot (\sin(Q\Delta\bar{x}), -\cos(Q\Delta\bar{x}), 0). \quad (25)$$

An electromagnetic field exerts a force on the bimeron that depends on its position relative to the spiral background $\Delta\bar{x}$. Neglecting second-order terms in $\alpha \ll 1$ and combining Eq. (12), Eq. (24), and Eq. (25), we get the equations of motion Eq. (13) and Eq. (14) for the bimeron under the action of a rotating magnetic field $\mathbf{H}(t) = |\mathbf{H}|(\cos(\omega t), \sin(\omega t), 0)$.

APPENDIX B: ATOMISTIC SPIN DYNAMICS SIMULATIONS

To support the analytical results, we perform various atomistic spin dynamics simulations using the UppASD code [27], which numerically solves the LLG equations, i.e. the equations of motion derived from Eq. (11), for a lattice model. Consequently, the numerical results do not involve the continuum approximation and the collective coordinates approach. Defining $\mathbf{m}_{\mathbf{r}}$ as the unit vector along the spin at the lattice site \mathbf{r} , the simplest lattice model described by Eq. (1) takes the form

$$H = \sum_{\mathbf{r}} (J_1 \mathbf{m}_{\mathbf{r}} \cdot \mathbf{m}_{\mathbf{r}+\hat{x}} + J_2 \mathbf{m}_{\mathbf{r}} \cdot \mathbf{m}_{\mathbf{r}+2\hat{x}} + J_{\perp} \mathbf{m}_{\mathbf{r}} \cdot \mathbf{m}_{\mathbf{r}+\hat{y}} + K_z (\mathbf{m}_{\mathbf{r}} \cdot \hat{z})^2 - \mu \mathbf{H} \cdot \mathbf{m}_{\mathbf{r}}) \quad (26)$$

with competing nearest neighbor $J_1 < 0$ and next nearest neighbor $J_2 > 0$ exchange interactions in the x -direction, ferromagnetic $J_{\perp} < 0$ in the y -direction, hard- z anisotropy $K_z > 0$, magnetic moment of a single spin μ and applied magnetic field \mathbf{H} . At $\mathbf{H} = 0$, the continuum limit of Eq. (26) is equivalent to Eq. (1) with $Q = \arccos(-J_1/4J_2)$ and $J_x = J_2 \sin^2 Q/Q^2$.

We first relax the bimeron Ansatz Eq. (4) with the following parameters: $J_1 = -1.4$ mRy, $J_2 = 0.38$ mRy, $J_{\perp} = -0.4$ mRy, $K_z = 0.008$ mRy, $\mu = \mu_B$ and $\alpha = 0.1$, where α denotes the Gilbert damping. The relaxed spin texture is qualitatively very similar to the Ansatz and

continues to obey the symmetries defined in Eq. (6) and Eq. (7). We then apply a rotating magnetic field \mathbf{H} in the xy -plane with $|\mathbf{H}| = 0.1$ T and angular frequency $\omega \in [0.25, 5]$ GHz. The results, shown in Fig. 3, are in excellent agreement with the analytical solution, Eq. (15) and Eq. (16), once $\hbar S = \hbar/2$ and the lattice constant $a = 0.5$ nm are restored. As predicted by Eq. (14), the bimeron also moves in the y -direction. The ratio between velocities along y and along x does not depend on ω and is approximately -21.6 with this choice of parameters. We perform a similar set of simulations with an antiferromagnetic $J_{\perp} > 0$ in the y -direction. The motion in the x -direction is equivalent to the previous case, with the critical frequency given by Eq. (22). However, the bimeron no longer moves along y in agreement with Eq. (21).

-
- [1] T. Skyrme, Nuclear Physics **31**, 556 (1962).
 - [2] A. M. Polyakov and A. A. Belavin, JETP Lett. **22**, 245 (1975).
 - [3] A. Bogdanov and A. Hubert, Journal of Magnetism and Magnetic Materials **138**, 255 (1994).
 - [4] N. Nagaosa and Y. Tokura, Nature Nanotechnology **8**, 899 (2013).
 - [5] A. Fert, V. Cros, and J. Sampaio, Nature nanotechnology **8**, 152 (2013).
 - [6] S. S. P. Parkin, M. Hayashi, and L. Thomas, Science **320**, 190 (2008).
 - [7] T. Kimura, T. Goto, H. Shintani, K. Ishizaka, T.-h. Arima, and Y. Tokura, Nature **426**, 55 (2003).
 - [8] H. Katsura, N. Nagaosa, and A. V. Balatsky, Phys. Rev. Lett. **95**, 057205 (2005).
 - [9] M. Mostovoy, Phys. Rev. Lett. **96**, 067601 (2006).
 - [10] F. Li, T. Nattermann, and V. L. Pokrovsky, Phys. Rev. Lett. **108**, 107203 (2012).
 - [11] F. Foggetti, M. Parodi, N. Nagaosa, and S. Artyukhin, Electric field-induced domain wall motion in spin spiral multiferroics (2024), arXiv:2204.09027 [cond-mat.str-el].
 - [12] L. Maranzana, N. Nagaosa, and S. Artyukhin, arXiv preprint arXiv:2403.11195 (2024).
 - [13] D. J. Gross, Nucl. Phys. B **132**, 439 (1978).
 - [14] Y. A. Kharkov, O. P. Sushkov, and M. Mostovoy, Phys. Rev. Lett. **119**, 207201 (2017).
 - [15] S. K. Kim, Phys. Rev. B **99**, 224406 (2019).
 - [16] X. Zhang, J. Xia, L. Shen, M. Ezawa, O. A. Tretiakov, G. Zhao, X. Liu, and Y. Zhou, Phys. Rev. B **101**, 144435 (2020).
 - [17] A. Pozzi and M. Mostovoy, Single-layer skyrmions in a van der waals antiferromagnet (2021), arXiv:2111.11420 [cond-mat.str-el].
 - [18] D. Bachmann, M. Lianeris, and S. Komineas, Phys. Rev. B **108**, 014402 (2023).
 - [19] W. Wang, M. Beg, B. Zhang, W. Kuch, and H. Fangohr, Phys. Rev. B **92**, 020403 (2015).
 - [20] K.-W. Moon, D.-H. Kim, S.-G. Je, B. S. Chun, W. Kim, Z. Q. Qiu, S.-B. Choe, and C. Hwang, Scientific Reports **6**, 20360 (2016).
 - [21] N. del Ser and V. Lohani, SciPost Phys. **15**, 065 (2023).

- [22] L. Shen, X. Li, J. Xia, L. Qiu, X. Zhang, O. A. Tretiakov, M. Ezawa, and Y. Zhou, Phys. Rev. B **102**, 104427 (2020).
- [23] N. del Ser, L. Heinen, and A. Rosch, SciPost Phys. **11**, 009 (2021).
- [24] D. Kurebayashi, Y. Liu, J. Masell, and N. Nagaosa, Phys. Rev. B **106**, 205110 (2022).
- [25] L. D. Landau and E. M. Lifshitz, Phys. Z. Sowjetunion **8**, 153 (1935).
- [26] T. L. Gilbert, IEEE Trans. Magn. **40**, 3443 (2004).
- [27] B. Skubic, J. Hellsvik, L. Nordström, and O. Eriksson, J. Phys.: Condens. Matter **20** (2008).
- [28] R. A. Duine, Lecture notes on spintronics (2010).
- [29] N. L. Schryer and L. R. Walker, J. Appl. Phys. **45**, 5406 (1974).
- [30] O. A. Tretiakov, D. Clarke, G.-W. Chern, Y. B. Bazaliy, and O. Tchernyshyov, Phys. Rev. Lett. **100**, 127204 (2008).
- [31] D. J. Clarke, O. A. Tretiakov, G.-W. Chern, Y. B. Bazaliy, and O. Tchernyshyov, Phys. Rev. B **78**, 134412 (2008).
- [32] P. Yan and X. R. Wang, Phys. Rev. B **80**, 214426 (2009).
- [33] D.-H. Kim, D.-H. Kim, D.-Y. Kim, S.-B. Choe, T. Ono, K.-J. Lee, and S. K. Kim, Phys. Rev. B **102**, 184430 (2020).
- [34] T. Hoffmann, P. Thielen, P. Becker, L. Bohatý, and M. Fiebig, Phys. Rev. B **84**, 184404 (2011).
- [35] T. Hoffmann, *Domain Patterns and Dynamics in the Magnetoelectric Switching of Spin-Spiral Multiferroics*, Ph.D. thesis, Rheinische Friedrich-Wilhelms-Universität Bonn (2013).
- [36] Y. Tokura and S. Seki, Advanced Materials **22**, 1554 (2010).
- [37] Q. Song, C. A. Occhialini, E. Ergeçen, B. Ilyas, D. Amoroso, P. Barone, J. Kapeghian, K. Watanabe, T. Taniguchi, A. S. Botana, S. Picozzi, N. Gedik, and R. Comin, Nature **602**, 601 (2022).
- [38] J. Sødequist and T. Olsen, 2D Mater. **10**, 035016 (2023).